AGU PUBLICATIONS

JGR

Journal of Geophysical Research: Oceans

RESEARCH ARTICLE

10.1002/2015JC011124

Special Section:
Forum for Arctic Modeling and Observational Synthesis (FAMOS): Results and Synthesis of Coordinated Experiments

Seasonal heat and freshwater cycles in the Arctic Ocean in CMIP5 coupled models

Yanni Ding[1], James A. Carton[1], Gennady A. Chepurin[1], Michael Steele[2], and Sirpa Hakkinen[3]

[1]Department of Atmospheric and Oceanic Science, University of Maryland, College Park, Maryland, USA, [2]Polar Science Center, Applied Physics Laboratory, University of Washington, Seattle, Washington, USA, [3]National Aeronautics and Space Administration, Goddard Space Flight Center, Greenbelt, Maryland, USA

Key Points:
- Explores the Arctic Ocean/ice seasonal heat and freshwater cycles in models
- Cycles in CMIP5 models are dominated by surface fluxes and/or storage
- Seasonal sea ice changes dominate both cycles and link them

Supporting Information:
- Supporting Information S1

Correspondence to:
J. A. Carton,
carton@atmos.umd.edu

Citation:
Ding, Y., J. A. Carton, G. A. Chepurin, M. Steele, and S. Hakkinen (2016), Seasonal heat and freshwater cycles in the Arctic Ocean in CMIP5 coupled models, *J. Geophys. Res. Oceans*, *121*, 2043–2057, doi:10.1002/2015JC011124.

Received 8 JUL 2015
Accepted 21 JAN 2016
Accepted article online 15 FEB 2016
Published online 1 APR 2016

Abstract This study examines the processes governing the seasonal response of the Arctic Ocean and sea ice to surface forcings as they appear in historical simulations of 14 Coupled Model Intercomparison Project Phase 5 coupled climate models. In both models and observations, the seasonal heat budget is dominated by a local balance between net surface heating and storage in the heat content of the ocean and in melting/freezing of sea ice. Observations suggest ocean heat storage is more important than sea ice melt, while in most of these models, sea ice melt dominates. Seasonal horizontal heat flux divergence driven by the seasonal cycle of volume transport is only important locally. In models and observations, the dominant terms in the basin-average seasonal freshwater budget are the storages of freshwater between the ocean and sea ice, and the exchange between the two. The largest external source term is continental discharge in early summer, which is an order of magnitude smaller. The appearance of sea ice (extent and volume) and also ocean stratification in both the heat and freshwater budgets provides two links between the budgets and provides two mechanisms for feedback. One consequence of such an interaction is the fact that models with strong/weak seasonal surface heating also have strong/weak seasonal haline and temperature stratification.

1. Introduction

The seasonal cycle is the largest signal in Arctic surface temperature with its annual swing, rivaling in magnitude the 20–30°C temperature changes associated with ice age climate transitions [*Alley*, 2000]. It is forced by a summer-time excess of surface shortwave radiation followed by an excess of longwave and turbulent heat loss in fall through early spring [*Serreze et al*., 2007]. The ocean/sea ice system plays a central role in moderating seasonal surface temperature changes by storing or releasing this heat between seasons. The seasonal cycle of freshwater, in contrast, is approximately independent of atmospheric hydrologic fluxes. While still poorly constrained by observations [*Serreze et al*., 2006], its budget appears to be dominated by seasonal exchanges between sea ice and the liquid ocean.

Proshutinsky et al. [2008] outlines a progression of stages by which we can use climate models to improve understanding and raise the possibility of climate prediction in the Arctic. The process begins with an exploration of the key balances in the models; progresses to identification of problems/uncertainties via model validations; identification of causes of the problems and recommendations for improvements. Already much work along these lines has been carried out with ocean general circulation models forced with specified atmospheric forcing (the Arctic Ocean Model Intercomparison Project) [e.g., *Johnson et al*., 2012]. This study represents an early effort to extend this effort to diagnose the processes regulating the seasonal heat and freshwater cycles of the Arctic Ocean to coupled models where the surface meteorology, ocean, and sea ice systems must all satisfy the dynamic and thermodynamic equations.

An important aspect of the scientific community effort to understand climate variability at high latitudes is the development and application of coupled climate models that must simulate these key processes. In this study, we examine the seasonal heat and freshwater budgets during the last half of the twentieth century in a recent suite of such models to explore similarities in their representations of the seasonal heat and freshwater cycles and the linkages between the two. The emphasis here is on discovery of intermodel similarities, i.e., one aspect of the first stage of model intercomparison discussed by *Proshutinsky et al*. [2008].

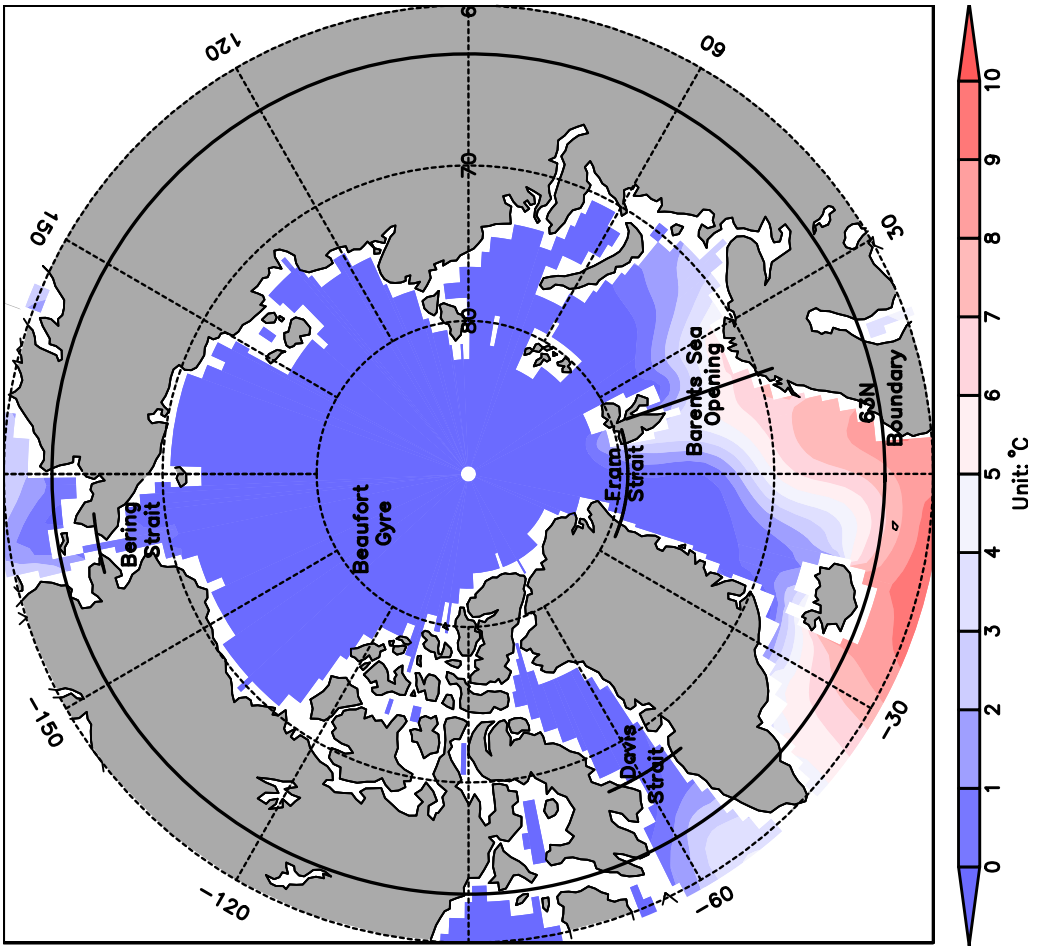

Figure 1. Mean upper layer (0–100 m) temperature from PHC3.0 (Polar Science Center Hydrographic Climatology version 3).

A distinguishing feature of the Arctic Ocean is the fact that it exchanges water with the Atlantic and Pacific only through a limited set of passages (Figure 1). Warm salty Atlantic Water flows into the Arctic basin through the Greenland, Iceland, and Norwegian Seas at a rate of 8 Sv (1 Sv = 10^6 m^3 s^{-1}) [*Yashayaev and Seidov*, 2015] with seasonal variations in temperature and salinity [*Furevik*, 2001]. Three to four Sverdrups of this flow continues northward into the central Arctic Ocean through the eastern side of Fram Strait while 2–3 Sv enters the Arctic Ocean through the Barents Sea Opening, the latter providing the heat necessary to keep the Barents Sea partially ice free even in winter [*Tsubouchi et al.*, 2012; *Smedsrud et al.*, 2013]. Some of this warming is evident in the distribution of annual mean (sea surface temperature) SST shown in Figure 1. An additional 0.5–1 Sv of cooler and fresher water enters the Arctic Basin from the Pacific with stronger flow in summer than winter [*Woodgate et al.*, 2005]. This inflow into the Arctic is balanced by cool water exiting the basin through the western side of Fram Strait as well as through Davis Strait. This outflow carries with it up to 0.2 Sv of sea ice, peaking in winter and early spring [*Kwok et al.*, 2004; *Spreen et al.*, 2009].

Seasonal variations of the Arctic Ocean heat budget are forced by the difference between net downwelling shortwave radiation and net upwelling longwave radiation and turbulent surface heat transfer. The ocean/sea ice system influences this exchange through the effects of SST and sea ice cover on latent, sensible, and longwave radiation and the effect of sea ice cover on surface albedo. This sea ice cover reaches a seasonal maximum extent of nearly 1.5 × 10^7 km^2 (based on the 1979–2000 average) in March, then decreases by a factor of 2 through summer and early fall [*Cavalieri et al.*, 2003]. This decline in sea ice cover lowers the average albedo of the Arctic Ocean and enhances the absorption of sunlight [*Perovich et al.*, 2008; *Steele et al.*, 2010; *Chan and Comiso*, 2013]. In midsummer when the sea ice cover is low, the net surface heating rate

approaches 100 W m^{-2} into the surface [*Serreze et al*., 2007]. In the transition season of summer/fall, *Serreze et al*. [2006] and *Steele and Flato* [2000] estimate that more than half of the surface heat that had been input during late spring through early fall goes to melting approximately 1 m of sea ice (using the heat flux numbers provided in *Serreze et al*. [2007, Table 2]). An additional smaller fraction of heat is absorbed by melting of the snow residing on sea ice. In the following seasons, this summer heat is lost to the atmosphere through longwave emission and latent and sensible heat exchanges, leading to ocean cooling and refreezing of the seasonal sea ice. Other terms in the heat balance such as seasonal changes in ocean heat transport divergence, sea ice export, and the thermal energy stored in sea ice, precipitation, and continental discharge are all smaller by a factor of 10 or more.

Like the seasonal cycle of heat, the seasonal cycle of freshwater in the Arctic is also primarily controlled by a balance local to the Arctic. The major freshwater exchange is between the salty ocean and the volume change of nearly fresh sea ice (salinities between 2 and 6 psu) during the melting/freezing cycle [*Kwok et al*., 2004; *Serreze et al*., 2006]. The involvement of seasonal sea ice as a major term in both the heat and freshwater budgets links these seasonal budgets together in a way that does not happen at lower latitudes. The seasonal cycles of heat and freshwater are both modulated by long-term changes in the seasonal sea level pressure field, notably the multiyear fluctuations in the strength of the Beaufort high and Icelandic low described by *Proshutinsky and Johnson* [1997] and *Polyakov et al*. [1999]. Changes in the strength and position of these features are associated with many meteorological changes including frequency and severity of storms, position of storm tracks, cloudiness, surface air temperature, and air humidity. The associated changes in the seasonal wind stress curl are able to alter the horizontal circulation in the ocean. When the Beaufort high is anomalously high, the surface circulation in the central Arctic becomes anticyclonic, and the surface salinity becomes smaller because more freshwater is concentrated in the Beaufort Gyre.

The Coupled Model Intercomparison Project has archived multiple generations of coupled model simulations with different models, the latest being Phase 5 (CMIP5) [*Taylor et al*., 2012]. This ensemble of simulations provides a rich source of information about the processes regulating the seasonal cycle of meteorological processes at high latitude and their impacts on changes in sea ice cover. The extensive meteorological literature includes the examination by *Svensson and Karlsson* [2011] of the atmospheric processes regulating wintertime air temperature in CMIP3 models, and the *Karlsson and Svensson* [2013] exploration of the role of surface albedo and cloud processes in regulating summer surface heating in a mixture of CMIP3 and CMIP5 models. These studies, along with the more recent studies by *Mortin et al*. [2014] and *English et al*. [2015], highlight the fact that most models are able to provide a reasonable simulation of the seasonal cycle of surface air temperature, while exhibiting variations in the magnitude of surface fluxes of tens of W m^{-2}.

The impact of net surface energy flux in regulating sea ice sea cover is also discussed in a number of these papers and others [e.g., *Stroeve et al*., 2012; *Wang and Overland*, 2012] due to the importance of net surface energy flux in balancing the latent heat of melting. In contrast to these essentially meteorological studies, there has been little attention directed toward the more poorly observed oceanic energy and freshwater cycles. For this reason, our emphasis in this initial study is to use the ensemble of simulations to focus on common features of the budgets, with less emphasis on exploring the differences among models. We begin by examining modeled surface fluxes in comparison with observational-based estimates, and then examine the resulting climatological monthly heat and freshwater cycles.

2. Data and Methods

We examine a total of 68 simulations from 14 CMIP5 models driven by historical records of greenhouse forcings and aerosols (the number of ensemble members for each model is given in parentheses): CanESM2 (5), CCSM4 (6), CNRM-CM5 (10), GFDL-CM3 (5), GFDL-ESM2G (2), GFDL-ESM2M (3), GISS-E2-R (6), HadCM3 (10), HadGEM2-ES (4), IPSL-CM5A-MR (3), MIROC5 (5), MPI-ESM-LR (3), MRI-CGCM3 (3), and NorESM1-M (3). Most models were obtained from the Program for Climate Model Diagnosis and Intercomparison, while some ensemble members of the two GFDL-ESM models were obtained directly from the Geophysical Fluid Dynamics Laboratory. A number of previous studies have evaluated meteorological variables and sea ice cover from these CMIP5 models at Arctic latitudes. Three of the models we examine, CanESM2, HadGEM2-ES, and IPSL-CM5A-MR, are categorized as "high performing" in the *Fyfe et al*. [2013] examination of Arctic

surface air temperature trends. *Wang and Overland* [2012] evaluated many of these models based on the realism of sea ice extent and found a different "best performing" set of models: CCSM4, HadGEM2-ES, MPI-ESM-LR, and MRI-CGCM3.

Vertical resolution varies among our ocean models with NorESM1-M having the finest vertical resolution (70 levels) and HadCM3 having the coarsest (20 levels). Most models have approximately 1° × 1° horizontal ocean resolution in midlatitudes except for IPSL-CM5A-MR, whose resolution is approximately 2° × 2°. All model output was obtained at monthly resolution. The calculations reported here are carried out separately on individual ensemble members and then averaged to form a monthly climatology for each model (averaging successive Januaries, Februaries, etc.), generally for the 46 year period 1957–2002. This period is sufficiently long that it averages the regime shifts described by *Proshutinsky and Johnson* [1997], but short enough to limit the effects of the decline of Arctic sea ice extent (see supporting information). The latter effects on the seasonal cycle are discussed in a separate study by *Carton et al*. [2015].

To evaluate the realism of the simulated seasonal surface fluxes, we follow *Serreze et al*. [2006, 2007] and compare our model fluxes to the ERA-40 reanalysis produced by the European Centre for Medium-Range Weather Forecasts (ECMWF), spanning the same 1957–2002 period [*Uppala et al*., 2005]. All atmospheric reanalysis face challenges in reproducing conditions in the Arctic [*Lindsay et al*., 2014]. Among the problems that have been identified for ERA-40 is that it has top-of-the-atmosphere radiation that is too large in summer and too small in fall and winter by 10 W m^{-2} or more [*Serreze et al*., 2007, and references therein] and has perhaps related issues with its representation of cloud cover [*Walsh and Chapman*, 1998; *Chan and Comiso*, 2013].

Initially we present some flux comparisons computed over an Arctic cap extending from the latitude of Iceland at 63°N–90°N. However, most of the geographic averages presented here are carried out in the Arctic Ocean domain of *Tsubouchi et al*. [2012], defined by major oceanographic passages into the central Arctic, enclosing an area 11.3 × 10^{12} m^2 (Figure 1). Our results are presented either as monthly averages or are further averaged into a summer (June–September) and winter season (December–March), with the definition of these seasons chosen as a compromise between the timing of solar forcing extrema and that of ocean and sea ice variables such as sea ice extent.

Monthly volume, heat, and freshwater horizontal transport terms for the ocean, snow, and sea ice are carried out on the original model grids for 10 of the models (requiring us to define the central Arctic domain slightly differently for each of these models due to differences in the numerical grids). The other four were only available on a remapped uniform grid rather than the native grids. Of the three transports, only volume transport can be computed accurately using monthly data, and even for volume transport, we were only able to reduce the residual for 11 of the models to within ±0.2 Sv (Table 1). For two models, HadGEM2-ES and MRI-CGCM3, the residual in summer was greater than 1 Sv exiting the basin and the residual in winter was less than 1 Sv entering the basin. These residuals are too large to be accounted for by unresolved terms such as sea ice export. For the fourteenth model, MIROC5, closure was not possible and so is not included in Table 1. Fortunately, the heat and freshwater transports are not among the dominant terms in their respective seasonal budgets (except locally).

The storage of heat and freshwater is calculated on a uniform 1° × 1° grid, constructed from the original model output using UNIDATA climate data operators (code.zmaw.de/projects/cdo). The seasonal heat storage is the time rate of change (computed from monthly differences) of ocean heat capacity, $HCO' = \rho_o C_p \int_{1500m}^{0} T' dz$, in units of W m^{-2}, where T' is the seasonal anomaly of temperature, ρ_o is ocean density, and C_p is heat capacity at constant pressure. The deep ocean below 1500 m depth is excluded from consideration, as there is essentially no seasonal variation at this depth [*Ding et al*., 2014]. Indeed, most of the seasonal variability is confined to the upper 100 m. For some models such as NorESM1-M, the mean vertical stratification is relatively weak, while in others such as GISS-E2-R, IPSL-CM5A-MR, and MRI-CGCM3, it is stronger than observed (supporting information Figure S1), which tends to extend or limit the depth of penetration of seasonal storage. In analogy to ocean heat storage, the sea ice latent heat storage is the time rate of change of sea ice latent heat capacity $HCI' = \rho_i L D'$, where ρ_i is the density of sea ice, L is the latent heat of melting (enthalpy of fusion), and D' is the change in sea ice thickness.

We compare simulated heat storage to observation-based estimates computed from the Polar Science Center Hydrographic Climatology version 3 (PHC3.0) analysis of historical hydrography [*Steele et al*., 2001]. PHC3.0 is based significantly on data collected in only two seasons: August–September or March–April

Table 1. Seasonal Volume Transports Through Bering, Davis, and Fram Straits, and Across the Barents Sea Opening in Summer (JJAS) and Winter (DJFM)[a]

	Bering Strait		Davis Strait		Fram Strait				Barents Sea Opening	
					JJAS		DJFM			
Models	JJAS	DJFM	JJAS	DJFM	EGC	WSC	EGC	WSC	JJAS	DJFM
CanESM2	1.1	0.9	0	0	−4.8	2.0	−5.1	1.8	1.8	2.5
CCSM4	1.1	1.1	−1.7	−1.8	−1.5	0.5	−3.2	1.2	1.6	2.7
CNRM-CM5	1.9	1	−2.6	−2.2	−2.2	0.7	−3.1	1.4	1.7	2.9
GFDL-CM3	1.2	0.9	−0.7	−0.7	−7.7	5.6	−8.6	6.0	1.4	2.3
GFDL-ESM2G	1.1	0.8	−1.1	−1.1	−5.7	4.8	−5.4	4.2	0.7	1.5
GFDL-ESM2M	1.1	0.8	−0.3	−0.4	−8.0	5.3	−9.1	6.1	1.8	2.4
GISS-E2-R	0.2	0.1	−0.2	−0.2	−1.4	1.0	−1.4	1.0	0.2	0.4
HadCM3	0	0	0	0	−7.5	6.4	−8.6	6.6	0.7	1.9
HadGEM2-ES	0.9	0.4	−0.8	−0.6	−5.2	1.1	−7.3	4.9	2	3
IPSL-CM5A-MR	1.5	1.2	−0.5	−0.5	−2.4	1.3	−2.4	0.9	0	0.7
MPI-ESM-LR	0.9	0.6	−1.3	−1.2	−10.8	8.7	−13.6	10.6	2.4	3.7
MRI-CGCM3	1	1.1	−1.2	−1	−4.4	1.3	−4.0	1.5	1.9	3
NorESM1-M	1.6	1.5	−1.9	−2.1	−10.4	9.0	−9.4	7.1	1.7	2.8
Observations	1.0[b]	0.5[b]	−1.4[c]		−1.7[c,d]				2.2[e]	1.9[e]

[a]See Figure 1 for approximate locations. Two components of the Fram Strait, East Greenland Current (EGC) and West Spitsbergen Current (WSC), are shown. Units are Sv. Volume transport balance closes to within ±0.3 Sv for each model in each season except for HadGEM2-ES and MRI-CGCM3. The contributions of net precipitation minus evaporation, river discharge, and sea ice export are smaller (observational estimates are given in *Serreze et al.* [2006] and are not included here.

[b]*Woodgate et al.* [2005], but note the presence of trends [*Woodgate et al.*, 2012].

[c]*Rudels et al.* [2008] annual average.

[d]Fram Strait transport is the result of two large opposing flows. *Beszczynska-Moller et al.* [2012] estimate the annual mean of the northward component to be 6.6 Sv, reaching a maximum of 9 Sv in March with a minimum of 4 Sv in July.

[e]*Smedsrud et al.* [2013].

[*Timokhov and Tanis*, 1997], with data collected mainly prior to the 1990s. *Serreze et al.* [2007] estimates the uncertainty in the climatological monthly heat content computed using PHC3.0 to be 2%, however, at least for the Beaufort gyre, observations show that the PHC3.0 climatology misses important semiannual variability [*Proshutinsky et al.*, 2009].

We also include an additional Arctic regional model [*Häkkinen and Mellor*, 1992; *Häkkinen*, 1999]. The regional model is a coupled ice-ocean model using Princeton Ocean Model numerics, covering the Arctic and the North Atlantic Oceans. The horizontal resolution is approximately 0.5° × 0.5° and there are 37 layers. Surface forcing is provided by the National Centers for Environmental Prediction reanalysis of *Kalnay et al.* [1996]. We also include estimates of seasonal heat and freshwater storage and associated changes in sea ice volume from the Pan-Arctic Ice Ocean Modeling and Assimilation System (PIOMAS) [*Zhang and Rothrock*, 2003], which uses the same surface forcing, but includes assimilation of sea ice extent and sea surface temperature.

Freshwater storage is calculated from column-averaged salinity following *Serreze et al.* [2006] as $-\int\int\int(dS/dt)\,S_{ref}{}^{-1}dv$ (where v is the volume of sea water in our domain) in units of Sv with $S_{ref}=34.7$ psu for PHC3.0. *Serreze et al.* [2006] provides a cautionary estimate of the freshwater content uncertainty of 10%, making even the seasonal cycle uncertain. The freshwater storage for the simulations is calculated using different values of S_{ref} to reflect differences in model average salinities (supporting information Figure S1). Seasonal freshwater transport has also been calculated from volume transport F_T as $F_{FW}=F_T(1-S/S_{ref})$ [*Serreze et al.*, 2006], however, these transport estimates are somewhat crude due to our use of monthly averaged fields, and so are referred to only in passing.

Seasonal sea ice extent is an important contributor to seasonal variations in surface heat flux. Here we compare simulated monthly sea ice extent to the National Snow and Ice Data Center (NSIDC) merged sea ice extent estimates (based on satellite microwave radiometer observations) spanning 1972–2002 [*Cavalieri et al.*, 2003].

3. Results

3.1. Surface Heat and Freshwater Flux

The seasonal cycle of surface heating is driven by annual variations in downwelling solar radiation whose phase is linked to the annual cycle of solar declination. For our Arctic cap spanning 63°N and 90°N, the

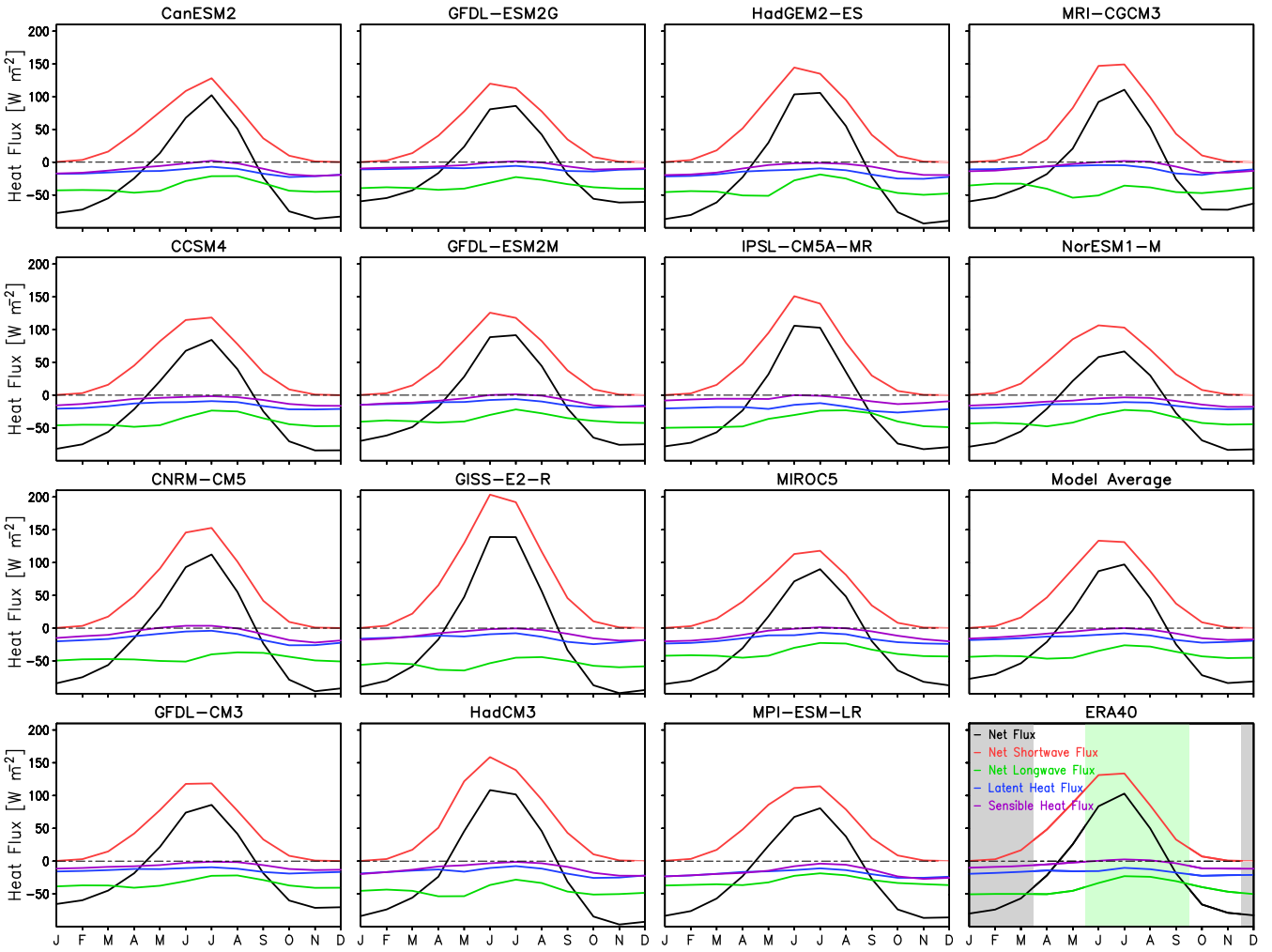

Figure 2. Seasonal cycle of surface heat flux (63°N–90°N), downward positive, computed over the 46 year period 1957–2002. Net shortwave (red), net longwave (green), latent (blue), sensible (purple), and net total (black) for models and reanalysis data (ERA-40).

observed monthly net shortwave flux at the surface reaches its maximum value of less than 150 W m^{-2} in July, which is after the summer solstice primarily due to changes in surface albedo (Figure 2, lower right). By September, the net surface flux has changed sign and from September to May, surface fluxes act to cool the Arctic.

The maximum monthly averaged net surface shortwave radiation in the models generally lies within ±25 W m^{-2} of the observations. The delay in net surface shortwave radiation relative to solar declination varies among models with a few models such as HadCM3 and GISS-E2-R showing less delay and an earlier switch in the sign of net surface flux. The remaining terms in seasonal surface heat flux, net longwave cooling, and the latent and sensible turbulent flux components have magnitudes of less than 50 W m^{-2} and all three act to cool the surface (Figure 2). Among these terms, sensible and net longwave cooling both increase in the winter months due to the cooler, dryer air and intensified winds in that season. The seasonal cycle of surface flux does not show many differences when the Arctic circulation pattern changes (supporting information Figures S6 and S7).

While the model-average surface fluxes are quite close to the ERA-40 reanalysis estimates, significant differences are apparent among individual models (Figure 2). GISS-E2-R, for example, has net peak shortwave radiation 50 W m^{-2}, higher than the model average. Examination of the surface downward and upward shortwave components separately shows that this model has both 30–40 W m^{-2} higher downward shortwave radiation than the model average and 20–30 W m^{-2} less upward shortwave radiation in July (Figure 3).

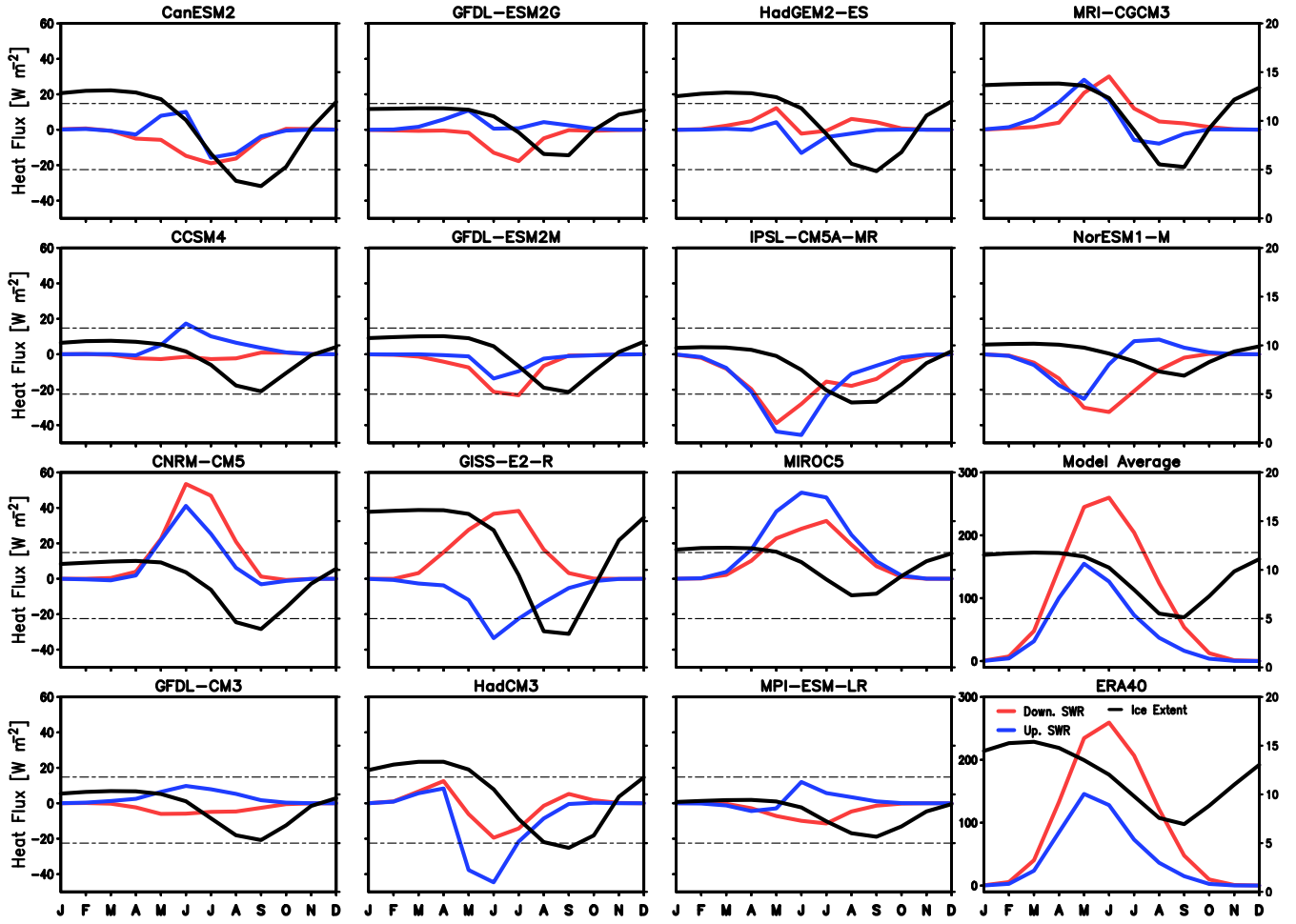

Figure 3. Seasonal cycle of the Arctic shortwave component anomaly (shortwave flux minus model-mean), computed over the 46 year period 1957–2002 for models and observations (ERA-40). Surface downward (red); surface upward (blue). Sea ice extent north of 63°N is also included (black).

The anomalously large downward radiation is due to the thin cloud cover (60% cloud fraction, at least 10% below the observational estimates of *Chan and Comiso* [2013]) in midsummer. The anomalously low upward shortwave radiation occurs despite the extensive early summer sea ice cover (Figure 3 and supporting information Figure S4) due to an unusually low value of sea ice albedo. The sea ice extent in this model undergoes a very dramatic decline in midsummer, reaching an average minimum of less than 5×10^6 km^2 by August–September. CNRM-CM5 has both higher than average downward and upward components, but the net flux is close to the model average. Finally, for the models with lower than average net shortwave radiation such as MIROC5, the higher than average upward shortwave radiation seems to be the result of unusually extensive summer sea ice cover (supporting information Figure S8).

The model-average cycle of surface freshwater flux is close to observations, with a peak in precipitation in September of 4 cm month^{-1}, a little above the observed estimate, rising from a minimum in May of 2.5 cm month^{-1} (Figure 4). Some particularly snowy models, such as HadGEM2-ES and IPSL-CM5A-MR, have summer maxima approaching 5 cm month^{-1}. Model average evaporation is highest in fall due to low sea ice cover, intensification of winds, and reduction in air humidity. The difference between precipitation and evaporation, which gives the net freshwater flux, is positive into the ocean, peaking at about 2 cm month^{-1} in August. This rate of net freshwater flux applied to our Arctic Ocean domain would result in a peak freshwater input of less than 0.1 Sv, while *Tsubouchi et al.* [2012] presents a single season estimate roughly twice as large. Continental discharge is only available for nine of the models. For these, the annual average varies between 0.04 and 0.12 Sv (supporting information Table S2). The latter, coming from MRI-CGCM3, more

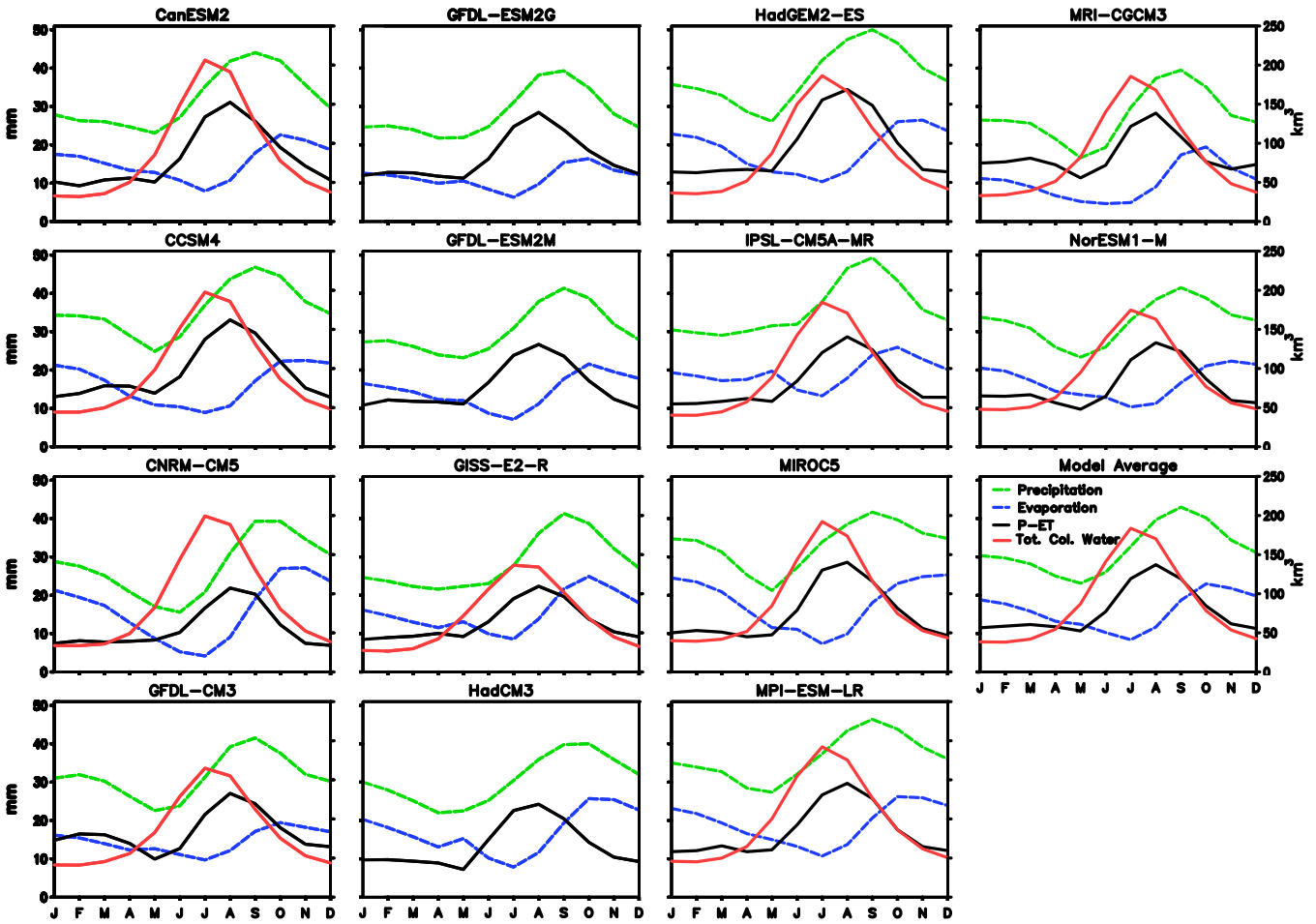

Figure 4. Seasonal cycle of surface freshwater flux into the ocean/sea ice (63°N–90°N), computed over the 46 year period 1957–2002 for models and observations (ERA-40). Precipitation (green), evaporation (blue), and total atmospheric water content (red).

closely approximates the estimates of *Serreze et al*. [2006]. Observed discharge peaks in June, in response to the contribution of continental snow and ice melt.

3.2. Seasonal Heat Balance

The seasonal storage in the ocean is largest in the Atlantic Sector south of Fram Strait where water remains ice free for much of the year (Figure 5). In the upper 100 m, the PHC3.0 climatology shows 1.5–2°C warmer temperatures in summer than winter, reflecting an increase in heat content of nearly 10^9 J m^{-2} in this sector. On average, the models store less heat in the ocean even though net surface heating is in line with the reanalysis estimate. The difference is likely due to larger sea ice cover in the models than observed and is most evident in generally icy models such as GFDL-ESM2G (supporting information Figure S4). The seasonal cycle of SST shows some limited and inconsistent changes with different Arctic circulation patterns (supporting information Figures S6 and S7).

Averaging over the ocean domain, the observed change in ocean heat storage reaches a maximum of +50 W m^{-2} in June and July, declining to a loss during late fall through early spring (Figure 6, lower right). Since this rate of storage is well below the rate of net surface heating of nearly 100 W m^{-2} and leads it by a month, other processes must be important. Turning to the model average seasonal heat budget, we see that latent heat of melting/freezing of sea ice accounts for both the missing heat input and the 1 month delay in net surface heating relative to the solar cycle. This means that other terms in the seasonal heat budget such as melting of snow, divergence of ocean transport, and warming of the ice itself are of secondary importance in the models (although they may play more of a role in the heat budget of the three GFDL

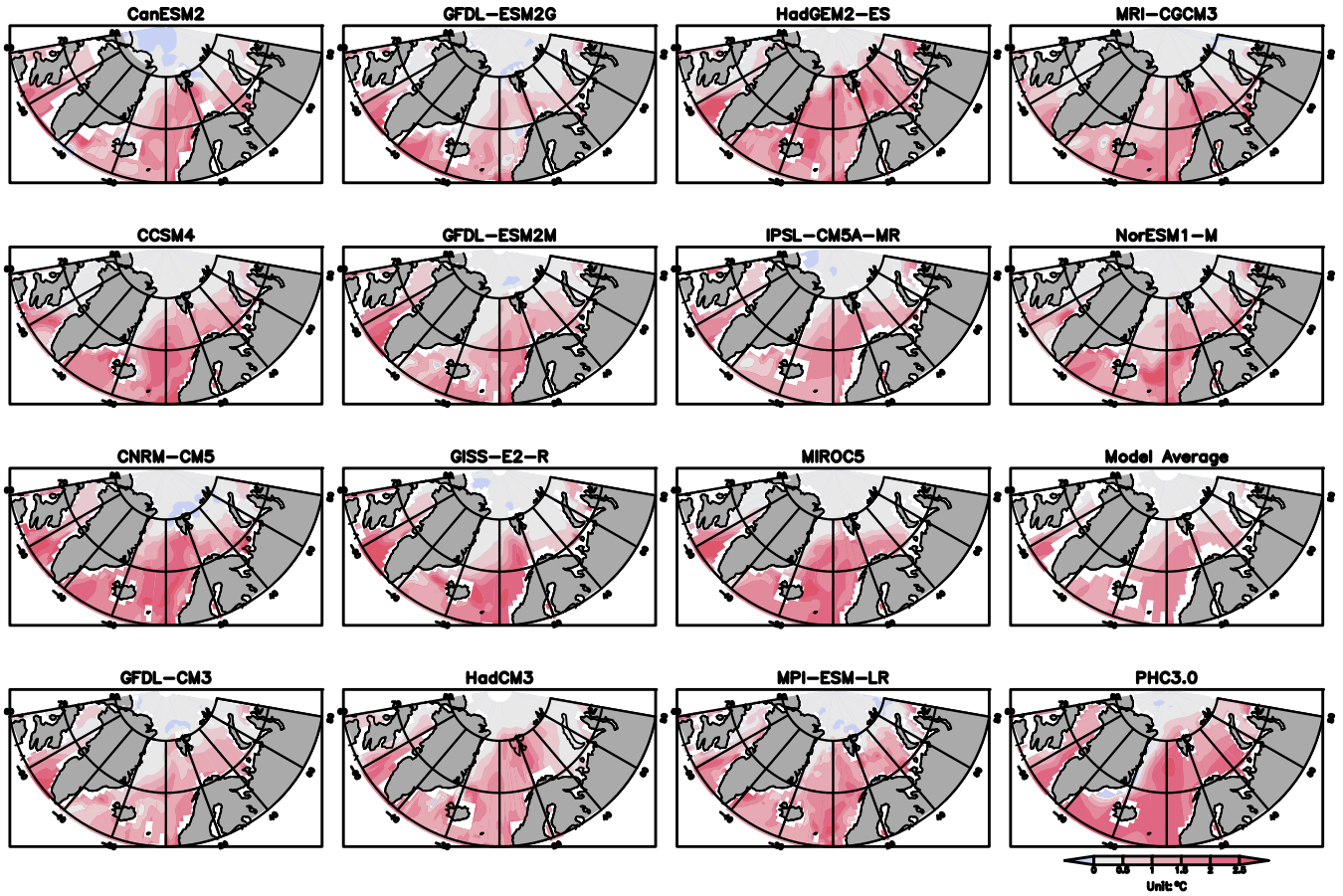

Figure 5. Seasonal change (summer (JJAS) minus winter (DJFM)) in upper ocean temperature (0–100m) computed over the period 1900–1994 for models and observations.

models). One exception is the model IPSL-CM5A-MR, for which the net surface heat input is 25 W m^{-2} larger than storage in summer.

If we assume that the same three-term balance that dominates the model heat budget applies to the observed ocean, then we can calculate the seasonal latent heat storage in sea ice. The result of this calculation is reassuringly close to the seasonal estimate produced by the PIOMAS sea ice reanalysis of *Zhang and Rothrock* [2003]. Interestingly, the model average seasonal ocean heat storage is significantly less than the seasonal heat stored in latent heat of melting of sea ice. This result is consistent with the study of *Zhang* [2005], but in disagreement with the estimates based on PHC3.0, and the regional model of *Häkkinen and Mellor* [1992]. Indeed, we note the latter has a significantly weaker seasonal cycle of heat storage than the CMIP5 models.

The success of the three-term balance for the seasonal heat budget averaged over the Arctic domain means that the basin-average contribution of seasonal heat transport convergence by ocean currents must be small. One reason for the relative weakness of this term is the compensating seasonal contributions by Bering Strait volume transport and Barents Sea Opening heat transport. Volume transport through Bering Strait strengthens in summer, bringing additional heat that is deposited in the Eurasian Arctic, leading to enhanced convergence of heat transport in summer (blue colors in Figure 7). In contrast, the Barents Sea remains ice free in winter causing huge heat transport convergence in this region in winter (red colors in Figure 7). Although the mean value of Atlantic inflow is much larger than the Pacific inflow, the amplitudes of their seasonal cycle are comparable. The two opposing seasonal differences may compensate with each other, as shown for CNRM-CM5 and HadGEM2-ES, and so limit the contribution of heat transport convergence averaged over the basin.

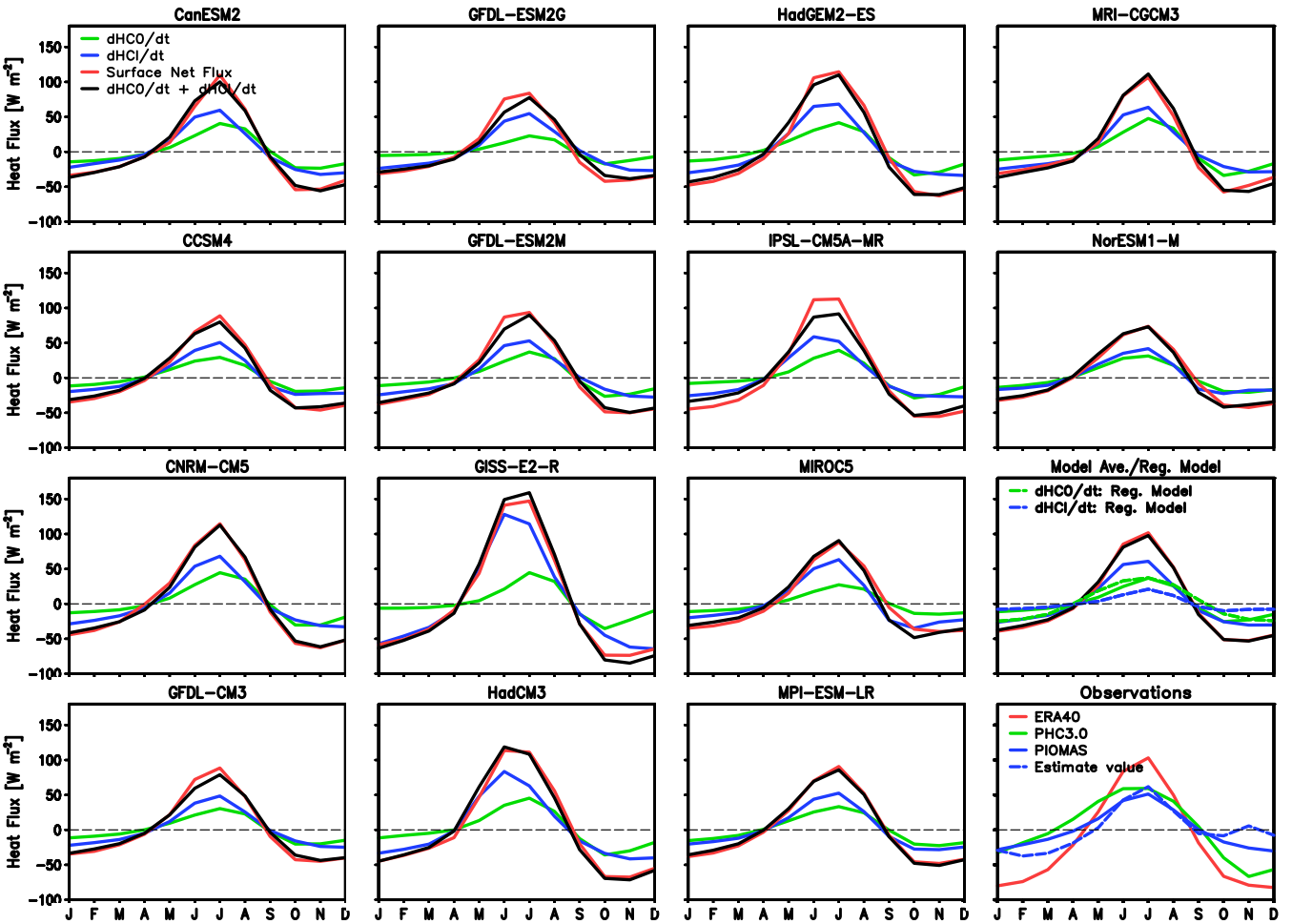

Figure 6. Seasonal heat budget of the Arctic Ocean (0–1500 m) computed over the 46 year period 1957–2002 for models and observations (ERA-40 and PHC3.0): ocean heat storage rate (∂HCO/∂t, green), sea ice heat storage rate (∂HCl/∂t, blue), and surface net flux (red). Results from regional model of *Häkkinen and Mellor* [1992] are shown in dash line in the second lowest plot on the right-hand side. In lowest right-hand plot, solid blue shows ∂HCl/∂t from PIOMAS (1979–2002) and dash blue is the calculated ∂HCl/∂t, which is a residual of observed heat flux and ocean heat storage.

3.3. Seasonal Freshwater Balance

We next examine the seasonal freshwater budget. Seasonal freshening of the ocean is most evident in the reduction in salinity in summer on the Eurasian and North American marginal seas as a result of both sea ice melt and the seasonal contributions of precipitation and river discharge (Figure 8). The model-average seasonal cycle is ∼50% weaker than PHC3.0 on the shelves and in the interior Arctic. This may reflect excess mixing or other model problems, but it also may reflect limitations of the observations due to a lack of observations in the central Arctic. The seasonal freshwater exchange between sea ice and ocean in the models reaches 2–3 Sv into the ocean in June and July (Figure 9), which is equivalent to a melt of ∼1 m of sea ice. The next largest term is continental discharge, during its peak in early summer when observations show the discharge rate may reach 0.4 Sv [*Serreze et al.*, 2006]. For most of the models, we consider, however, continental discharge is lower than observed by at least a factor of two. Finally, net precipitation minus evaporation is not an important contributor in the basin average. There are significant differences among the models in their seasonal cycle of salinity (Figure 9). CMIP5 models with relatively weak seasonal cycles of sea ice such as NorESM1-M, MIROC5, GFDL-CM3, and CCSM4 and the *Häkkinen and Mellor* [1992] regional model have quite weak seasonal cycles of salinity. In contrast, models with strong seasonal cycles of sea ice volume such as GISS-E2-R and HadCM3 have unusually strong seasonal cycles of salinity. In some models, like CCSM4 and NorESM1-M, the seasonal cycle of salinity is delayed, which might be a result of other freshwater fluxes like continental discharge and sea ice export.

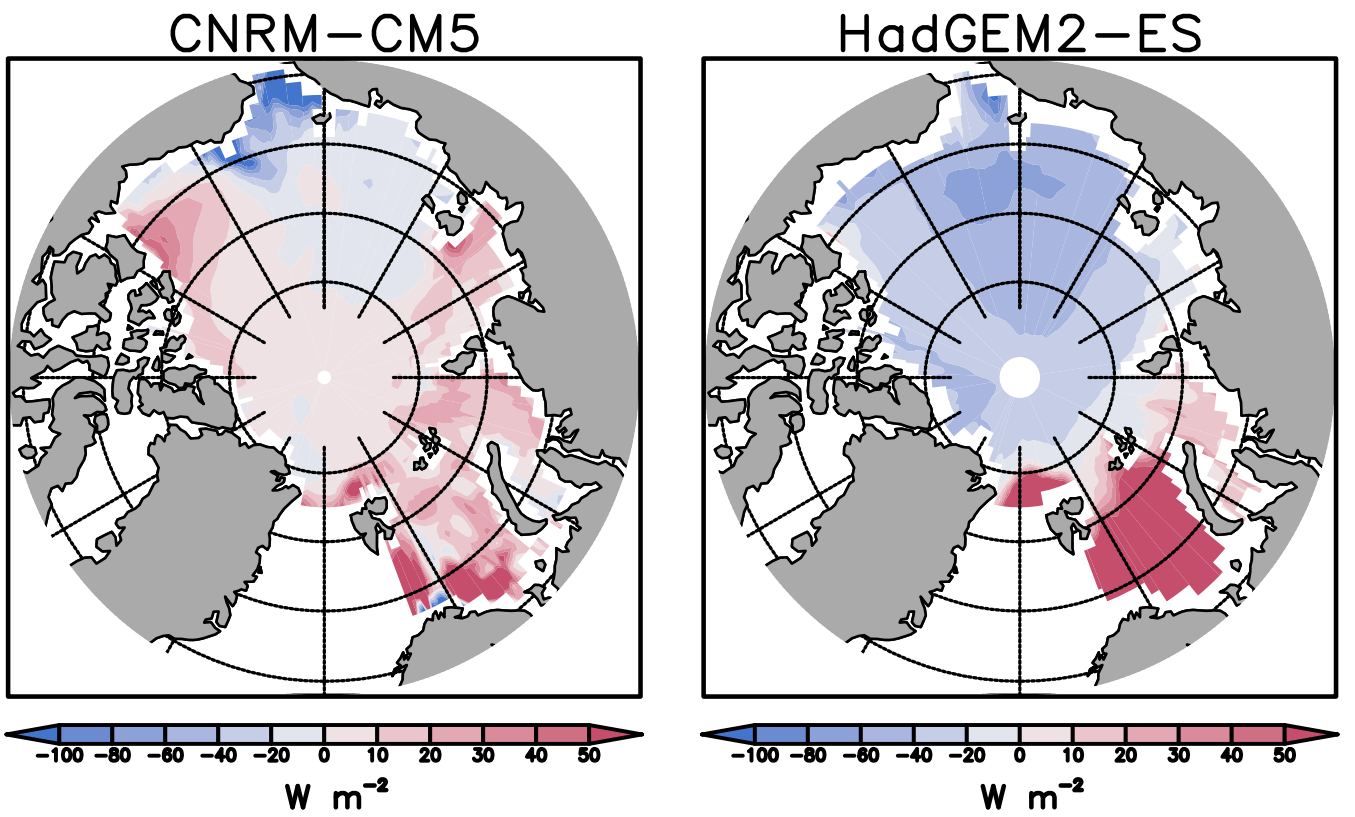

Figure 7. Seasonal change (summer (JJAS) minus winter (DJFM)) in ocean heat transport divergence calculated as the residual between surface net flux and local heat storage for two models with the large seasonal cycles of volume flux through the Bering Strait: CNRM-CM5 and HadGEM2-ES. The bright red areas highlight the ocean convergence of heat in the Barents Sea in winter.

4. Summary and Conclusions

Here we examine the late twentieth century seasonal heat (energy) and freshwater budgets of the Arctic Ocean as represented in historical simulations of a set of 14 CMIP5 coupled models. There are several reasons why it is interesting to explore these budgets. The first is that the budgets represent a key test of model physics, particularly the processes controlling the seasonal growth of sea ice. The second is that the observational record is uncertain, particularly in the case of the freshwater budget [e.g., *Serreze et al*., 2006], and the model results may help interpret the observational record. Such coupled models make an interesting complement to the higher-resolution Arctic Ocean Model Intercomparison Project coupled ocean-sea ice models [*Proshutinsky et al*., 2011], for which the surface fluxes are out of balance with the ocean properties. The third is that anticipated changes to the seasonal cycle in the coming centuries put a high priority on understanding dependencies, such as the relationship between the seasonal cycle and the mean state stratification.

The models considered here show that excess heat entering the ocean/sea ice system in summer is stored in the form of melting sea ice and to a lesser extent in increases in ocean temperature. The relationship between seasonal SST and seasonal surface air temperature is affected by the insulating effects of the areal extent of sea ice cover, which insulates the ocean below it, as well as mean stratification, which reduces vertical exchange. These two seasonal storage terms vary in phase and when summed together nearly balance net surface heat flux, consistent with observations [*Serreze et al*., 2007]. In contrast, seasonal heat transport convergence by ocean currents, the heat gain associated with seasonal ice export, and other terms like the heat associated with precipitation are small except in geographically limited areas. One such area may be the Barents Sea. *Mahlstein and Knutti* [2011] point out that some models retain excess summer sea ice in the Barents due to unrealistically weak inflows of warm Atlantic Water. Here we also find some low transport models which lose their sea ice because excess net surface heating compensates for the lack of ocean

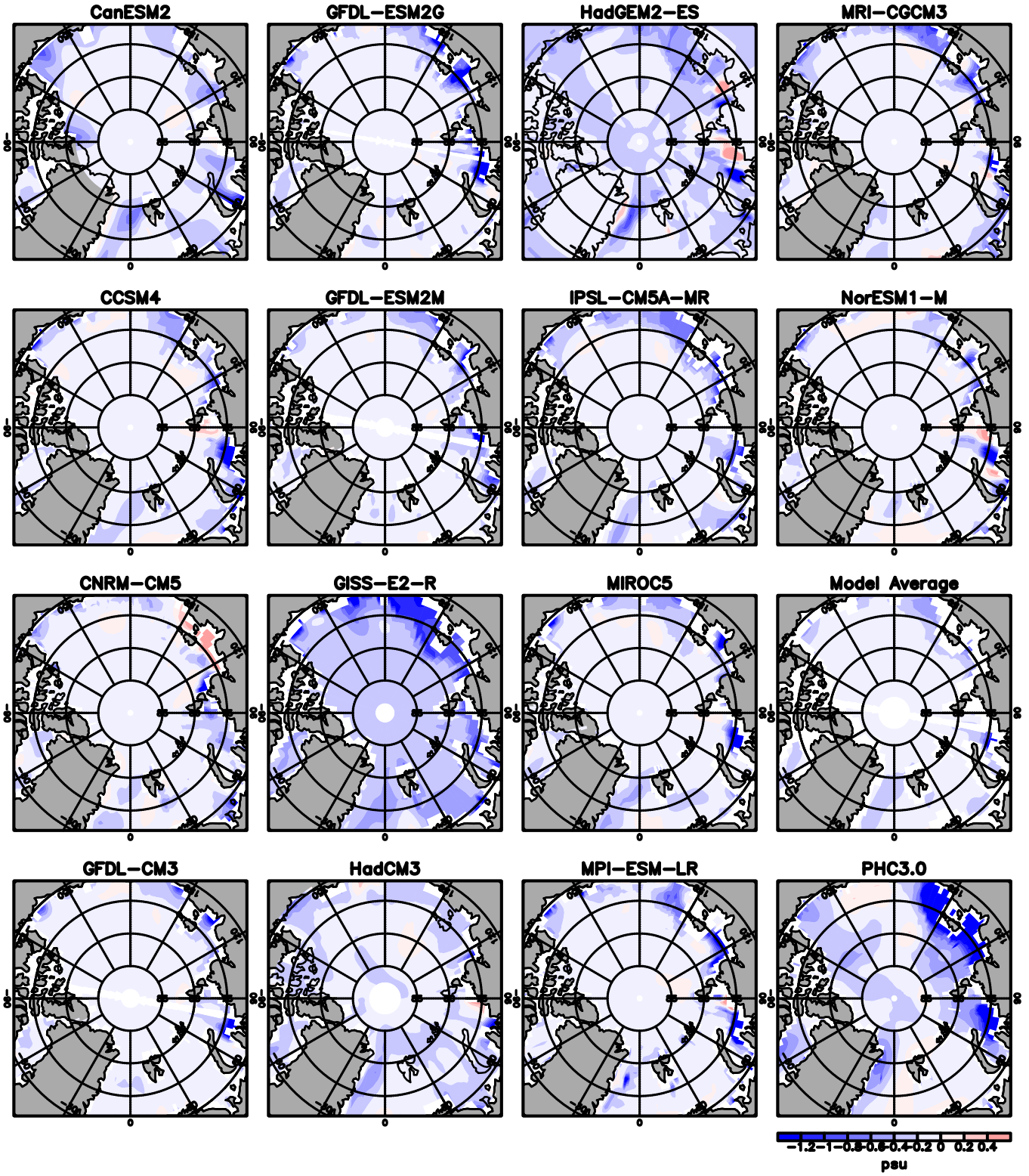

Figure 8. Seasonal change (summer (JJAS) minus winter (DJFM)) in upper layer salinity (0–100m) computed over the period 1900–1994 for models and observations.

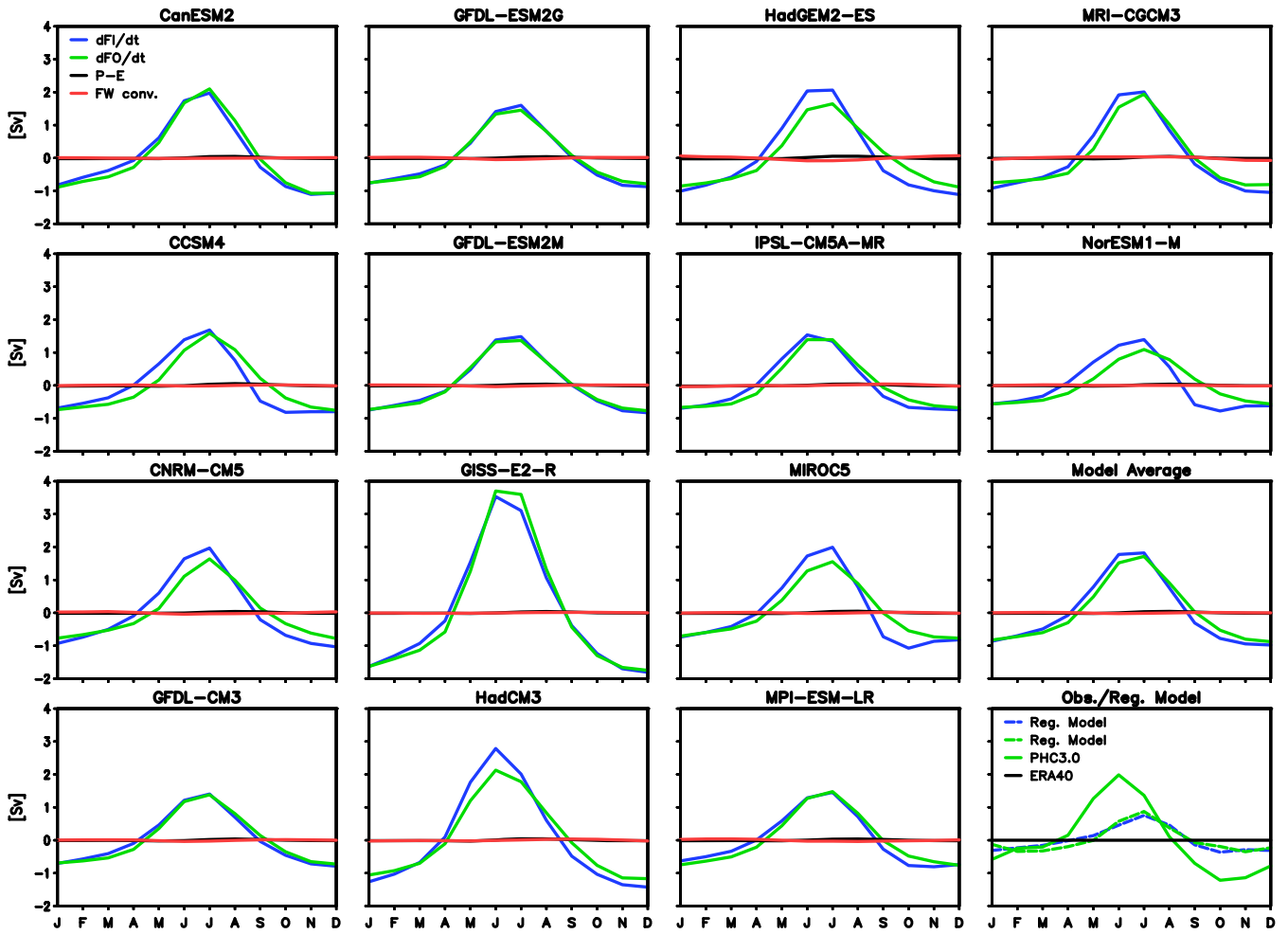

Figure 9. Seasonal freshwater budget of the Arctic Ocean (0–1500 m) for CMIP5 models, the Arctic regional model and observations: ocean freshwater storage rate ($\partial FO/\partial t$) in blue, sea ice freshwater storage rate ($-\partial FI/\partial t$) in green, P-E in black, and freshwater flux convergence in red. All are computed over from 1900 to 1994 except for ERA40, which is calculated from 1957 to 2002.

heat transport convergence. Compared to the observations and the regional model of *Häkkinen and Mellor* [1992], more heat is stored in the sea ice and less stored in the ocean heat content in CMIP5 models (probably a result of the larger sea ice volume in these models). The wide variety in the sea ice extent/volume highlights a problem with the CMIP5 models which needs to be addressed.

The magnitudes of seasonal freshwater storage in the liquid ocean and in sea ice are similar, but are nearly out of phase. The sum of the remaining terms, including net surface water flux, continental discharge, and sea ice export, is either negligible (in some models), or act to delay the seasonal storage in the ocean by a month or less (in others). This delaying effect is due to a combination of the spring peaks in three terms: continental discharge, sea ice export, and liquid ocean freshwater convergence, and their declines in fall.

The dominant role that seasonal sea ice areal extent and volume plays in both the heat and freshwater budgets causes interesting feedbacks between the two budgets. For example, strong/weak seasonal surface heating alters sea ice volume leading to strong/weak seasonal haline stratification, which in turn is able to strengthen/weaken the seasonal cycle of SST, further altering sea ice volume. One large perturbation that we can anticipate is the rapid decline in sea ice extent and volume during this century. As the decline progresses, the seasonal cycles of heat and freshwater must be altered fundamentally. What changes will occur and what their impacts will be on lower latitudes and on related systems such as biological production remain key open questions [*Carton et al.*, 2015].

Acknowledgments
Y.D., G.A.C., and J.A.C. gratefully acknowledge support from the National Science Foundation (OCE1233942). Support for M.S. was provided by NSF grant OCE1233255. We thank the World Climate Research Program's Working Group on Coupled Modeling, which is responsible for CMIP, and the climate modeling groups for producing and making available their model output. For CMIP, the U.S. Department of Energy's Program for Climate Model Diagnosis and Intercomparison (www-pcmdi.llnl.gov) provides coordinating support and led development of software infrastructure in partnership with the Global Organization for Earth System Science Portals. We thank the Geophysical Fluid Dynamics Laboratory for providing output from the two GFDL-ESM models used here. We thank the ECMWF, NSIDC, and PSC teams for the ERA-40 atmospheric fluxes, sea ice extent, PHC3.0 ocean climatology, and PIOMAS sea ice volume data. ERA-40 data were downloaded from http://apps.ecmwf.int/datasets/data/era40-moda/in 2014. The sea ice extent was downloaded from http://nsidc.org/data/on February 2014. The PHC3.0 ocean climatology was downloaded from http://psc.apl.washington.edu/nonwp_projects/PHC/ on October 2013. The PIOMAS data were downloaded from http://psc.apl.uw.edu/research/projects/arctic-sea-ice-volume-anomaly/data/on May 2015. We thank the support from Forum for Arctic Modeling and Observational Synthesis (FAMOS).

References

Alley, R. B. (2000), Ice-core evidence of abrupt climate changes, *Proc. Natl. Acad. Sci. U. S. A.*, *97*, 1331–1334, doi:10.1073/pnas.97.4.1331.

Carton, J. A., Y. Ding, and K. R. Arrigo (2015), The seasonal cycle of the Arctic Ocean under climate change, *Geophys. Res. Lett.*, *42*, 7681–7686, doi:10.1002/2015GL064514.

Cavalieri, D. J., C. L. Parkinson, and K. Y. Vinnikov (2003), 30-Year satellite record reveals contrasting Arctic and Antarctic decadal sea ice variability, *Geophys. Res. Lett.*, *30*(18), 1970, doi:10.1029/2003GL018031.

Chan, M. A., and J. C. Comiso (2013), Arctic cloud characteristics as derived from MODIS, CALIPSO, and CloudSat, *J. Clim.*, *26*, 3285–3306, doi:10.1175/JCLI-D-12-00204.1.

Ding, Y., J. A. Carton, G. A. Chepurin, G. Stenchikov, A. Robock, L. T. Sentman, and J. P. Krasting (2014), Ocean response to volcanic eruptions in Coupled Model Intercomparison Project 5 simulations, *J. Geophys. Res. Oceans*, *119*, 5622–5637, doi:10.1002/2013JC009780.

English, J. M., A. Gettelman, and G. R. Henderson (2015), Arctic Radiative Fluxes: Present-day biases and future projections in CMIP5 models, *J. Clim.*, *28*, 6019–6038.

Furevik, T. (2001), Annual and interannual variability of Atlantic Water temperatures in the Norwegian and Barents Seas: 1980–1996, *Deep Sea Res., Part I*, *48*, 383–404.

Fyfe, J. C., K. Von Salzen, N. P. Gillett, V. K. Arora, G. M. Flato, and J. R. McConnell (2013), Variability and trends of air temperature and pressure in the maritime Arctic, *Sci. Rep.*, *3*, 2645.

Häkkinen, S. (1999), Variability of the simulated meridional heat transport in the North Atlantic for the period 1951–1993, *J. Geophys. Res.*, *104*, 10,991–11,007.

Häkkinen, S., and G. L. Mellor (1992), Modeling the seasonal variability of a coupled Arctic ice-ocean system, *J. Geophys. Res.*, *97*, 20,285-20,304.

Johnson, M., et al. (2012), Evaluation of Arctic sea ice thickness simulated by Arctic Ocean Model Intercomparison Project models, *J. Geophys. Res.*, *117*, C00D13, doi:10.1029/2011JC007257.

Kalnay, E., et al. (1996), The NCEP/NCAR 40-year reanalysis project, *Bull. Am. Meteorol. Soc.*, *77*, 437–471.

Karlsson, J., and G. Svensson (2013), Consequences of poor representation of Arctic sea-ice albedo and cloud-radiation interactions in the CMIP5 model ensemble, *Geophys. Res. Lett.*, *40*, 4374–4379, doi:10.1002/grl.50768.

Kwok, R., H. Zwally, and D. Yi (2004), ICESat observations of Arctic sea ice: A first look, *Geophys. Res. Lett.*, *31*, L16401, doi:10.1029/2004GL020309.

Lindsay, R., M. Wensnahan, A. Schweiger, and J. Zhang (2014), Evaluation of seven different atmospheric reanalysis products in the Arctic, *J. Clim.*, *27*, 2588–2606.

Mahlstein, I., and R. Knutti (2011), Ocean heat transport as a cause for model uncertainty in projected Arctic warming, *J. Clim.*, *24*, 1451–1460.

Mortin, J., R. G. Graversen, and G. Svensson (2014), Evaluation of pan-Arctic melt-freeze onset in CMIP5 climate models and reanalyses using surface observations, *Clim. Dyn.*, *42*, 2239–2257.

Perovich, D. K., J. A. Richter-Menge, K. F. Jones, and B. Light (2008), Sunlight, water, and ice: Extreme Arctic sea ice melt during the summer of 2007, *Geophys. Res. Lett.*, *35*, L11501, doi:10.1029/2008GL034007.

Polyakov, I. V., A. Y. Proshutinsky, and M. A. Johnson (1999), Seasonal cycles in two regimes of Arctic climate, *J. Geophys. Res.*, *104*, 25,761–25,788.

Proshutinsky, A., K. Dethloff, R. Doescher, J. C. Gascard, and F. Kauker (2008), Toward reducing uncertainties in Arctic climate simulations, *Eos Trans. AGU*, *89*, 150–152.

Proshutinsky, A., R. Krishfield, M. L. Timmermans, J. Toole, E. Carmack, F. McLaughlin, W. J. Williams, S. Zimmermann, M. Itoh, and K. Shimada (2009), Beaufort Gyre freshwater reservoir: State and variability from observations, *J. Geophys. Res.*, *114*, C00A10, doi:10.1029/2008JC005104.

Proshutinsky, A., et al. (2011), Recent advances in Arctic Ocean studies employing models from the Arctic Ocean Model Intercomparison Project, *Oceanography*, *24*, 102–113.

Proshutinsky, A. Y., and M. A. Johnson (1997), Two circulation regimes of the wind-driven Arctic Ocean, *J. Geophys. Res.*, *102*, 12,493–12,514.

Serreze, M. C., A. P. Barrett, A. G. Slater, R. A. Woodgate, K. Aagaard, R. B. Lammers, M. Steele, R. Moritz, M. Meredith, and C. M. Lee (2006), The large-scale freshwater cycle of the Arctic, *J. Geophys. Res.*, *111*, C11010, doi:10.1029/2005JC003424.

Serreze, M. C., A. P. Barrett, A. G. Slater, M. Steele, J. Zhang, and K. E. Trenberth (2007), The large-scale energy budget of the Arctic, *J. Geophys. Res.*, *112*, D11122, doi:10.1029/2006JD008230.

Smedsrud, L. H., et al. (2013), The role of the Barents Sea in the Arctic climate system, *Rev. Geophys.*, *51*, 415–449, doi:10.1002/rog.20017.

Spreen, G., S. Kern, D. Stammer, and E. Hansen (2009), Fram Strait sea ice volume export estimated between 2003 and 2008 from satellite data, *Geophys. Res. Letts.*, *36*, L19502, doi:10.1029/2009GL039591.

Steele, M., and G. M. Flato (2000), Sea ice growth, melt, and modeling: A survey, in *The Freshwater Budget of the Arctic Ocean*, pp. 549–587, Springer, Dordrecht, Netherlands.

Steele, M., R. Morley, and W. Ermold (2001), PHC: A global ocean hydrography with a high-quality Arctic Ocean, *J. Clim.*, *14*, 2079–2087.

Steele, M., J. Zhang, and W. Ermold (2010), Mechanisms of summertime upper Arctic Ocean warming and the effect on sea ice melt, *J. Geophys. Res.*, *115*, C11004, doi:10.1029/2009JC005849.

Stroeve, J. C., M. C. Serreze, M. M. Holland, J. E. Kay, J. Malanik, and A. P. Barrett (2012), The Arctic's rapidly shrinking sea ice cover: A research synthesis, *Clim. Change*, *110*, 1005–1027.

Svensson, G., and J. Karlsson (2011), On the Arctic wintertime climate in global climate models, *J. Clim.*, *24*, 5757–5771.

Taylor K. E., R. J. Stouffer, and G. A. Meehl (2012), An Overview of CMIP5 and the Experiment Design, *Bull. Amer. Meteor. Soc.*, *93*(4), 485–498, doi:10.1175/BAMS-D-11-00094.1.

Timokhov, L., and F. Tanis (Eds.) (1997), *Joint U.S.-Russian Atlas of the Arctic Ocean [CD-ROM]*, Environ. Res. Inst. of Mich., Ann Arbor.

Tsubouchi, T., S. Bacon, A. C. Naveira Garabato, Y. Aksenov, S. W. Laxon, E. Fahrbach, A. Beszczynska-Möller, E. Hansen, C. M. Lee, and R. B. Ingvaldsen (2012), The Arctic Ocean in summer: A quasi-synoptic inverse estimate of boundary fluxes and water mass transformation, *J. Geophys. Res.*, *117*, C01024, doi:10.1029/2011JC007174.

Uppala, S. M., et al. (2005), The ERA-40 re-analysis, *Q. J. R. Meteorol. Soc.*, *131*, 2961–3012.

Walsh, J. E., and W. L. Chapman (1998), Arctic Cloud–Radiation–Temperature Associations in observational data and atmospheric reanalyses, *J. Clim.*, *11*, 3030–3045.

Wang, M., and J. E. Overland (2012), A sea ice free summer Arctic within 30 years: An update from CMIP5 models, *Geophys. Res. Lett.*, *39*, L18501, doi:10.1029/2012GL052868.

Woodgate, R. A., K. Aagaard, and T. J. Weingartner (2005), Monthly temperature, salinity, and transport variability of the Bering Strait throughflow, *Geophys. Res. Lett.*, *32*, L04601, doi:10.1029/2004GL02188.

Yashayaev, I., and D. Seidov (2015), The role of the Atlantic Water in multidecadal ocean variability in the Nordic and Barents Seas, *Prog. Oceanogr.*, *132*, 68–127.

Zhang, J. (2005), Warming of the arctic ice-ocean system is faster than the global average since the 1960s, *Geophys. Res. Lett.*, *32*, L19602, doi:10.1029/2005GL024216.

Zhang, J., and D. A. Rothrock (2003), Modeling global sea ice with a thickness and enthalpy distribution model in generalized curvilinear coordinates, *Mon. Weather Rev.*, *131*, 681–697.